Photogrammetric 3D reconstruction of Apollo 17 Station 6: From boulders to lunar rock samples integrated into virtual reality

Stéphane Le Mouélic, Mélanie Guenneguez, Harrison H. Schmitt, Louis Macquet, Nicolas Mangold, Gwénaël Caravaca, Benoît Seignovert, Erwan Le Menn, Laurent Lenta

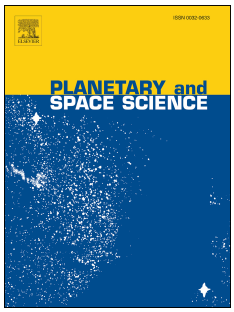

Photogrammetric 3D reconstruction of Apollo 17 Station 6: From boulders to lunar rock samples integrated into virtual reality

S. Le Mouélic, M. Guenneguez, H.H. Schmitt, L. Macquet, N. Mangold, G. Caravaca, B. Seignovert, E. Le Menn, L. Lenta

PII: S0032-0633(23)00182-4

DOI: https://doi.org/10.1016/j.pss.2023.105813

Reference: PSS 105813

To appear in: *Planetary and Space Science*

Received Date: 18 August 2023

Revised Date: 9 October 2023

Accepted Date: 17 November 2023

Please cite this article as: Le Mouélic, S., Guenneguez, M., Schmitt, H.H., Macquet, L., Mangold, N., Caravaca, G., Seignovert, B., Le Menn, E., Lenta, L., Photogrammetric 3D reconstruction of Apollo 17 Station 6: From boulders to lunar rock samples integrated into virtual reality, *Planetary and Space Science* (2023), doi: https://doi.org/10.1016/j.pss.2023.105813.

Photogrammetric 3D Reconstruction of Apollo 17 Station 6: From boulders to lunar rock samples integrated into virtual reality

S. Le Mouélic[1], M. Guenneguez[1], H. H. Schmitt[2], L. Macquet[1], N. Mangold[1], G Caravaca[3], B. Seignovert[4], E. Le Menn[1], L. Lenta[1]

[1]LPG, UMR CNRS 6112, Nantes Université, Univ. Angers, Univ. Le Mans, France.

[2]Dept of Engineering Physics, Univ. Wisconsin-Madison, P.O. Box 90730, Albuquerque, NM 87199, USA.

[3] IRAP, UMR 5277 CNES, UPS, CNRS, Toulouse, France.

[4]OSUNA, Nantes, France.

Corresponding Email : stephane.lemouelic@univ-nantes.fr

Full postal address : Laboratoire de Planétologie et Géosciences, CNRS UMR 6112, Nantes Université, Université d'Angers, Le Mans Université, Nantes, France,

Keywords: Moon, photogrammetry, lunar sample, Apollo, geology, virtual reality

Abstract

Apollo 17 astronauts spent three days exploring the Taurus Littrow Valley on the Moon in 1972. During their third Extravehicular Activity, they spent more than one hour at Station 6, a geologic waypoint consisting of three big and two small fragments of a boulder that rolled down the North massif. We have used all the available scanned digital Apollo photos taken by the astronauts at this Station 6 to compute a comprehensive 3D model of the explored area. We used Structure From Motion photogrammetry to automatically derive the position of each of the 154 available images using their overlap. All images were aligned in a single photogrammetric project, which allows on one hand to automatically visualize the astronaut positions during their investigations, and on the other hand to reconstruct in 3D the three main pieces of boulders, therefore constraining their respective size and orientation. In addition to the boulders, we show that the 3D reconstruction by photogrammetry can also be applied to the rock samples taken from the boulders themselves. These samples were systematically photographed from multiple angles at the LPI during the 70s when brought back to Earth. For the reconstruction, we used scanned archived images representing 16 stereoscopic pairs, to compute 3D models of samples 76015, 76215, 76315 and 76275. These models might play a role in preservation as some of the samples, latter sawed for analysis, do not exist anymore in their pristine form. 3D models of the boulders and rock samples can then be manipulated and visualized on a web-based platform. 3D models have also been integrated into a virtual reality scene in order to provide the possibility to investigate their properties at full scale in an immersive and collaborative way. The knowledge of the samples position and orientation directly in their context might for example provide additional constrains to better understand processes such as the space weathering alteration due to micrometeorite impacts and solar wind particle. 3D photogrammetric reconstructions using images taken by rovers and/or astronauts might be one of the basic techniques to consider in forthcoming lunar missions in order to maximize their scientific, educational and outreach return.

1- Introduction

The Apollo 17 mission landed in the Taurus Littrow valley on the Moon, December 11, 1972. The geology of the landing site, on the eastern edge of Mare Serenitatis, was thoroughly investigated during extra vehicular activities performed during a total of three days spent at the surface (Wolfe et al., 1981; Schmitt et al., 2017; Schmitt, 2023). 111 kg of representative rock and soil samples were collected, documented photographically and verbally, and brought back to Earth during this last Apollo mission. These samples also were carefully documented in the Lunar Receiving Lab facility in Houston. Among several geological waypoints of interest at Taurus Littrow, astronauts spent more than one hour investigating five large boulder fragments at a place called "Station 6", lying at the base of a long boulder trail descending from the North Massif (Figure 1). The boulder had rolled down a 22.5-degree slope forming a 10-m-wide trail that begins 394 m above and ends at the boulder's present location, where it had broken apart into five major pieces (Haase et al., 2019). The analysis by Schmitt et al. (2017) indicates that original single boulder originated in Crisium-age melt breccia ejecta overlain by Serenitatis-age melt breccia ejecta. Earlier photo geologic interpretations had suggested that the North Massif was largely Serenitatis in age (Spudis and Ryder 1981; Hurwitz and Kring, 2016).

In a previous study (Le Mouélic et al., 2020), we used scanned photographs taken *in situ* with astronaut's Hasselblad cameras to reconstruct individual 3D models of each of the main boulders of Station 6 using Structure from Motion photogrammetry techniques (Ullman, 1979; Favalli et al., 2012). Other studies used photogrammetric analysis of Apollo 11, 12 data (Pustynski and Jones, 2014; Pustynski 2021) mostly to relocate Apollo images. Photogrammetry was also used on Chang'E-4 rover images to produce a centimeter-resolution 3D model of craters and rocks of the landing site (Wu et al., 2020). In the first step presented in Le Mouélic et al. (2020), we showed that the photogrammetric 3D reconstruction of the individual boulders at Stations 2, 6 and 7 was possible, even if the images were taken 50 years ago with film photographs. However, in this first work, boulders were analyzed independently of each other. Their respective position and orientation at Station 6 was therefore not constrained with respect to each other's, and we did not consider the rock samples either. In the present study, we push the reconstruction process one step further first by using more photographs as input to better constrain the respective positioning and scaling of the main fragments of boulders at Station 6 in their global context, and second by applying the same photogrammetric technique to the rock samples themselves. We show in the first section that additional images such as the two 360° panoramas and images taken from the Lunar Roving Vehicle viewpoint can be integrated into a global photogrammetric project to cover the complete Station 6 area. In the second section, following up on the work of Wolfe, et. al. (1981), we show that the photogrammetric reconstruction process can be applied to several rock samples from Station 6, using original laboratory photography's of these rocks acquired several decades ago before they were sawed in several pieces for analysis. In the third section, we describe how the 3D models can be integrated in augmented and virtual reality, and we discuss the scientific implications of the complete 3D reconstruction of the boulders and rock samples to investigate, for example, the onset of phenomena such as the space weathering processes and local shadowing.

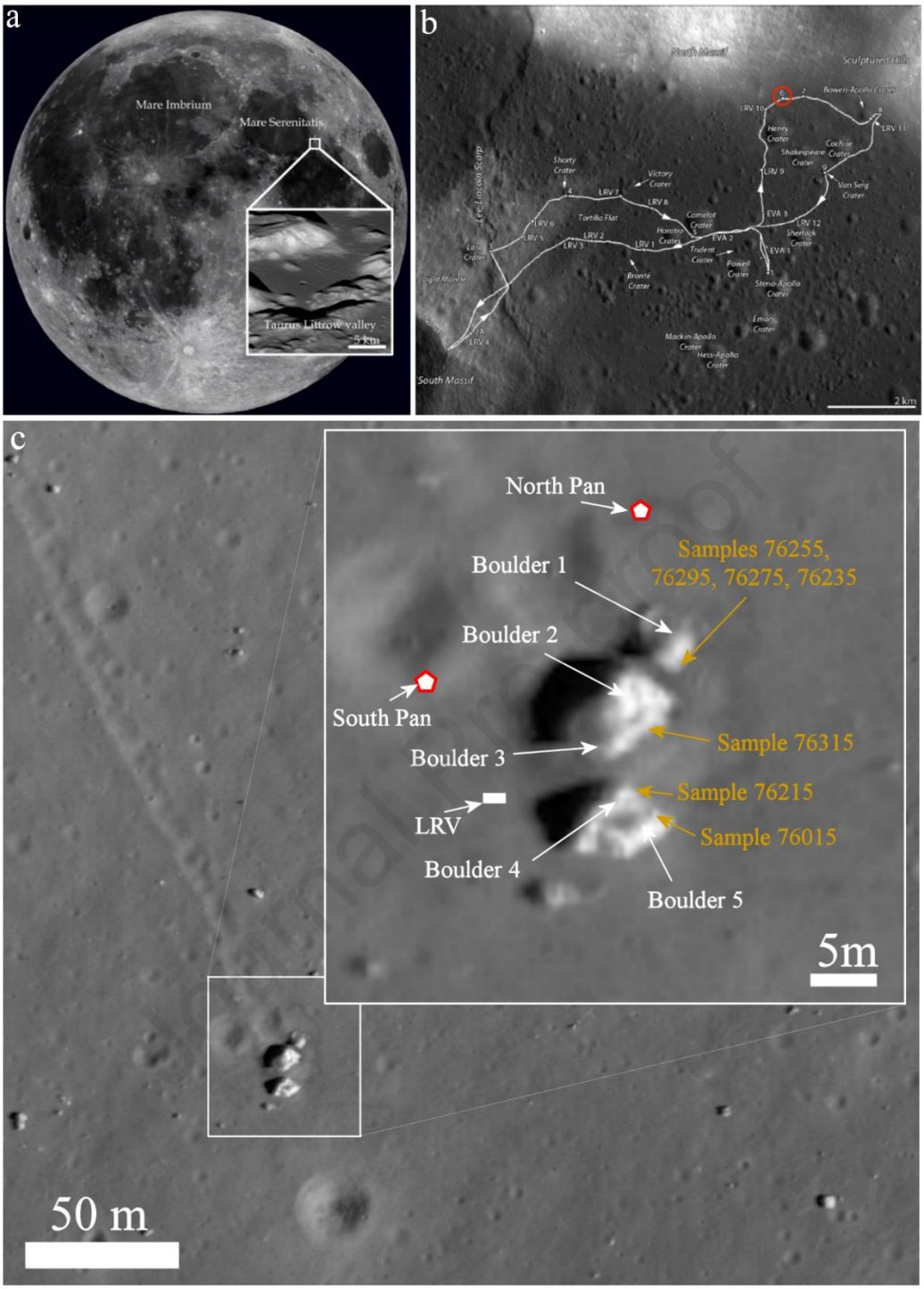

Figure 1: (a) Location of Taurus Littrow Valley. (b) Traverse map of the Extra Vehicular Activities. Station 6 (red circle) is located near the bottom of the south-facing slope of the North Massif (image adapted from LRO/ASU/R. Wagner). (c) LROC image of the boulder complex, showing the five major blocks at Station 6, and taken with the same lighting as during EVA-3 on December 13, 1972 (NAC image M129086118LR). Markings left by the astronauts in the soil are still visible on the right part of the boulders. The inset shows the boulders numbering, the temporary location of the Lunar Roving Vehicle and the approximate photometric positions of two 360° panoramas, with arrows pointing on the approximate rock sample locations.

2- Photogrammetric reconstruction of Station 6 boulders

2.1 3-D Reconstruction of individual boulders using Structure from Motion

In the previous Le Mouélic et al. (2020) study, we used the scanned version of the Apollo film photographs collection to carry out a photogrammetric reconstruction of individual boulders at Stations 2, 6 and 7, using the

Agisoft Metashape software. At Station 6, we reconstructed the individual boulders numbered 1, 2-3 and 4-5 (see the inset of Figure 1 for their location) using the Structure from Motion (SfM) technique (Ullman, 1979) on a total of 82 images. The spatial coverage, images overlap and number of viewpoints was indeed sufficient to enable an automatic reconstruction with SfM. In this SfM approach, series of tie points are automatically found using the correlation between pairs of images taken from different viewpoints. The parallax effect allows the derivation of the position of the tie points into the 3D space. Individual images are aligned by the algorithm at their respective position. After the first tie points and image alignment process, a dense cloud of matching points is created. Then, a polygonal mesh matching the dense cloud is computed. The final step consists in creating a texture corresponding to a mosaic of the original images, draped over the polygonal mesh. The full process is illustrated in Figure 2 (a to d) for Boulder 1.

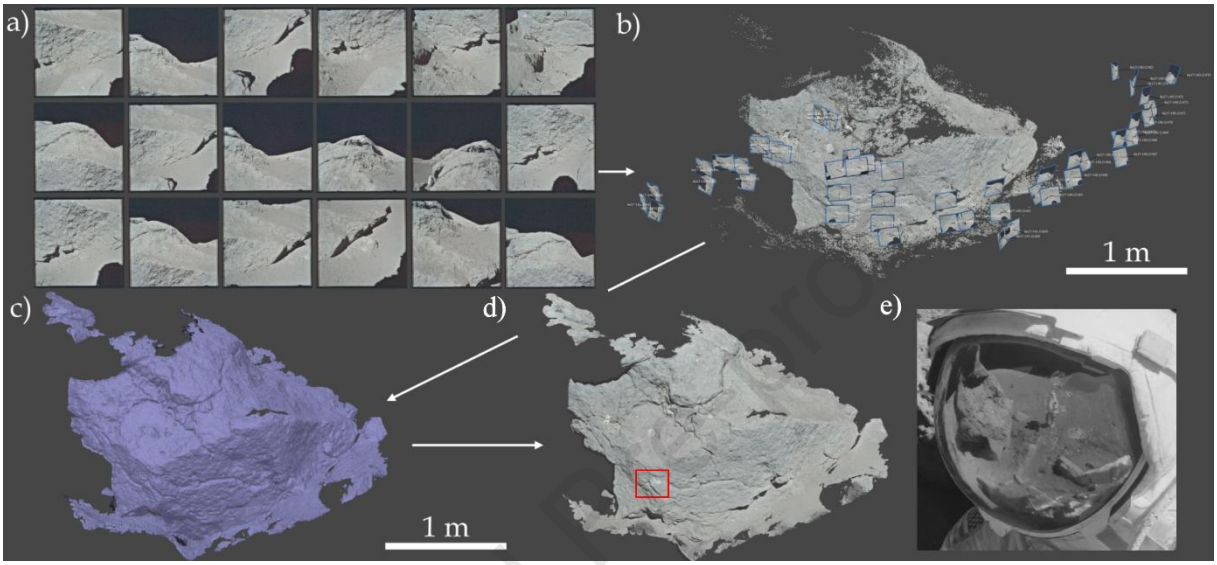

Figure 2: Photogrammetric reconstruction process for Boulder 1. (a) Subset of the original series of scanned Apollo photographs. (b) Tie points cloud and images aligned by the photogrammetric software. (c) polygonal mesh connecting the dense point cloud. (d) Final textured 3D model of boulder 1. The red rectangle highlights the area latter discussed in Fig. 15 (e) Subset of image As17-141-21608 showing the only available global view of Boulder 1, reflected in the helmet visor of Gene Cernan.

The astronauts took no global view of the southern face of Boulder 1 during the photographic documentation campaign. Only one indirect global view is fortuitously available, thanks to the reflection seen in Gene Cernan's helmet visor in image As17-141-21608, acting like a fish eye objective (Figure 2e). A generally good match between the photogrammetric reconstruction and the shape of Boulder 1 seen in this reflection is observed. In the study carried out in Le Mouélic et al. (2020), the main boulders of Station 6 were investigated independently of each other using respectively 42 (Boulder 1), 7 (Boulder 2-3) and 33 (Boulder 4-5) images. This left uncertainties about their respective position, scale and orientation. In the following section, we seek to overcome these shortcomings by adding more images as input to reconstruct the Station 6 area as a whole, in the same photogrammetric project, now using all the available 154 images instead of 82.

2.2 Comprehensive integration of the main pieces of boulders at Station 6

We have refined the original individual 3D models of the Station 6 boulders described in Le Mouélic et al. (2020) by adding in the photogrammetric project images of the two 360° panoramas taken from "North pan" (frames As17-140-21483-21508) and "South pan" (frames AS17-141-21575-21603). We have also added the two photographs As17-146-22293 and As17-146-22294 taken from the Lunar Roving Vehicle location parked in the South West of the site (see Figure 1c for their location and Figure 3 for corresponding added images). Five other images As17-141-21616-21620 provide a close up view of Boulder 2-3. Three images As17-141-21630 covering its back side (in complete shadow) were not included, due to a strong lack of contrast.

The 154 images were taken by two different cameras, each mounted on the chest of an astronaut. We made a preliminary test trying to separate the two data sets in Agisoft Metashape, but this did not seem to help in the alignment process, so we continued the process with no distinction between the two cameras, considering also the fact that the data set and images overlap were already quite sparse. The Hasselblad HDC cameras were equipped

with very high-quality Zeiss Biogon 60 mm f/5.6 lenses, custom-designed for use on the lunar surface, and calibrated to the reseau plate in the camera (Borgeson and Batson, 1969; Kuehnel, 1972). All lenses were designed with minimal tangential and radial distortions across the image field. We therefore made the assumption that they are similar at first order, when compared to other sources of variations such as the ones possibly induced by the scans of the negatives for example. We did not have access to optical parameters of the cameras, so the camera parameters were left free in Agisoft Metashape, with no self-calibration.

Several markers were added in the project in order to iteratively converge into a complete alignment of the set of 154 images (Figure 4). Images from the two 360° panoramas provide tie points that strongly constrain the respective position of boulders. Images taken from the LRV also provide views of the unlit backsides of the boulders, with enough recognizable tie points. The frame As17-140-21434 is the main key to link Boulders 2-3 with Boulder 4. It should be noted that there is only a very small overlap between images of the lit face of Boulders 2-3 and other boulders at Station 6. This might introduce some residual mismatch of the overall position or orientation, that we were not able to quantify. The integration of all these additional viewpoints in the same photogrammetric project, containing now a total of 154 aligned photographs instead of 82, still allowed a better absolute scaling and positioning of the five main boulders and part of the underlying ground. A total of one million tie points and a dense cloud of 110 million points was used to produce a textured mesh of 6 million polygons, which was reduced to 1.5 million polygons with 10 textures of 8192x8192 pixels to facilitate the manipulation of the final 3D product (Figure 5). On the final Agisoft Metashape project, the 981 204 tie points exhibit a reprojection residual error (RMS) of 1.18 pixels.

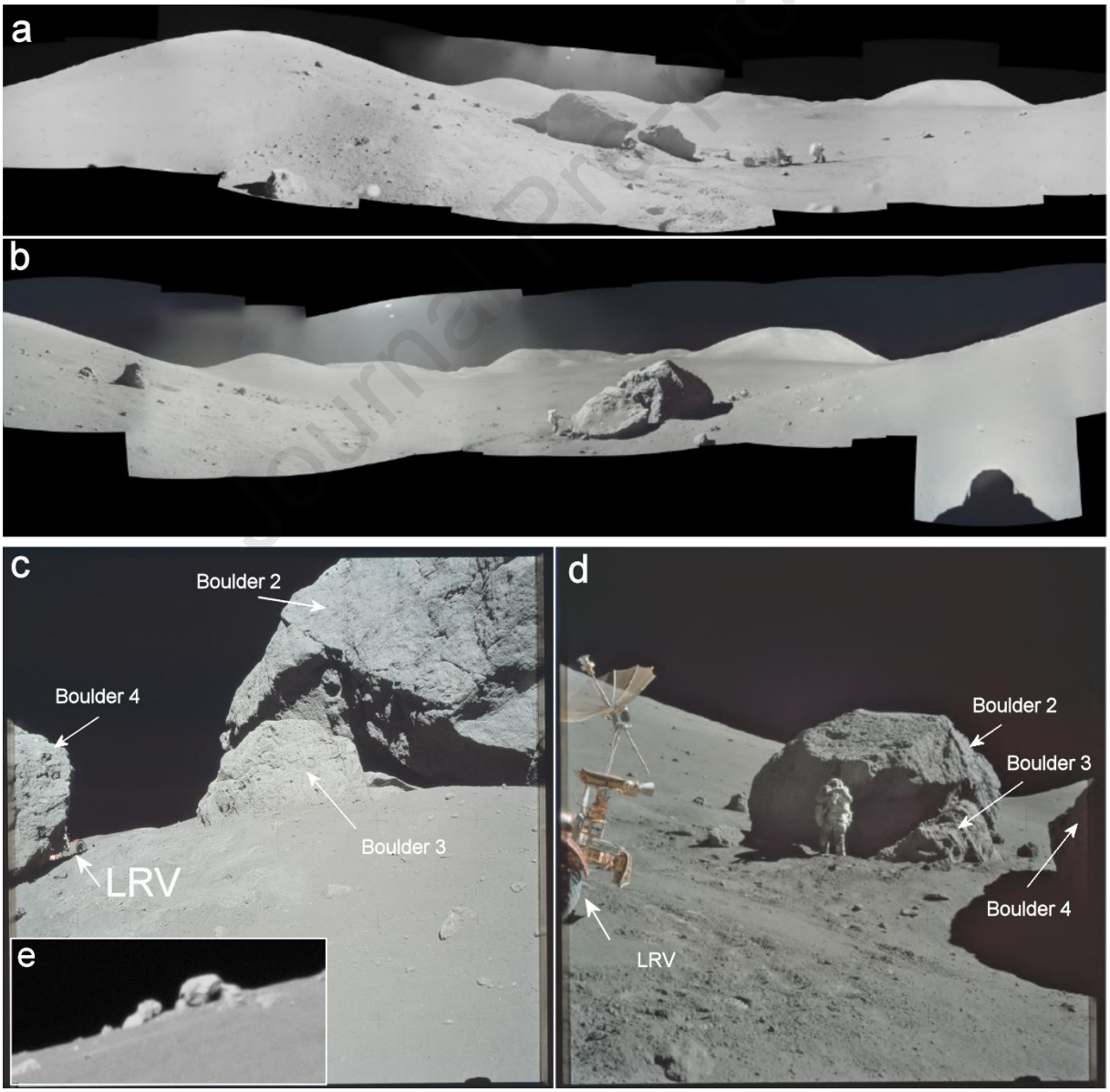

Figure 3: Panoramas and images added in the photogrammetric project to complement the 82 individual boulders images used in Le Mouélic et al. (2020). (a) "South" Panorama (frames AS17-141-21575-21603), (b) "North" Panorama (frames As17-

140-21483-21508). (c) frame As17-140-21434. The LRV is seen in the background behind boulder 4. This frame is the only one showing the lit side of Boulders 2-3 (in the upper right corner) with a partt of Boulder 4 (on the left). (d) Frame taken from the LRV showing the backside of boulder 2-3 and the edge of Boulder 4 (in shadow). (e) Subset of image AS17-146-22355 showing Station 6 as seen from Station 7, from a distance of 475m. A total of 154 aligned images is now used in the photogrammetric project to reconstruct Station 6 boulders (Figure 4).

The scaling of the different elements in the photogrammetric project can be constrained by the size of the astronaut's footprints, the gnomon (62 cm height when deployed (Allton, 1989)), the LRV, the position of the different cameras (located on the astronaut's chest, so with a constant height with respect to the ground) and the matching with LRO orbital imagery, which provides the general context. On the global perspective view from top (upper part of Figure 4), we see that the photogrammetric alignment process derived from the matching points in images pairs potentially allows a relocation of the position of the astronauts during their photographic campaign. Each of the 154 images is represented by a blue rectangle seen in perspective. These positions are at first order in good agreement with other independent investigations such as the Spatio-temporal maps of Roseborough et al. (2023), even if small differences can exist depending on the method used. In particular, positions of Gene A. Cernan at the 360° North Pan and Harrison H. Schmitt at the 360° South Pan appear thanks to the automated correlation process.

Jones et al. (2017) mention that the fragments of the Station 6 boulders can also be identified in image As17-146-22355 taken from Station 7, so from a distance of about 475m. According to the spacing of 10.3° of the reseau crosses, one can estimate from Station 7 that the separation of the tops of boulders 2 and 5 to be about ~9.7m (Jones et al., 2017). This estimation is compatible with our sizing.

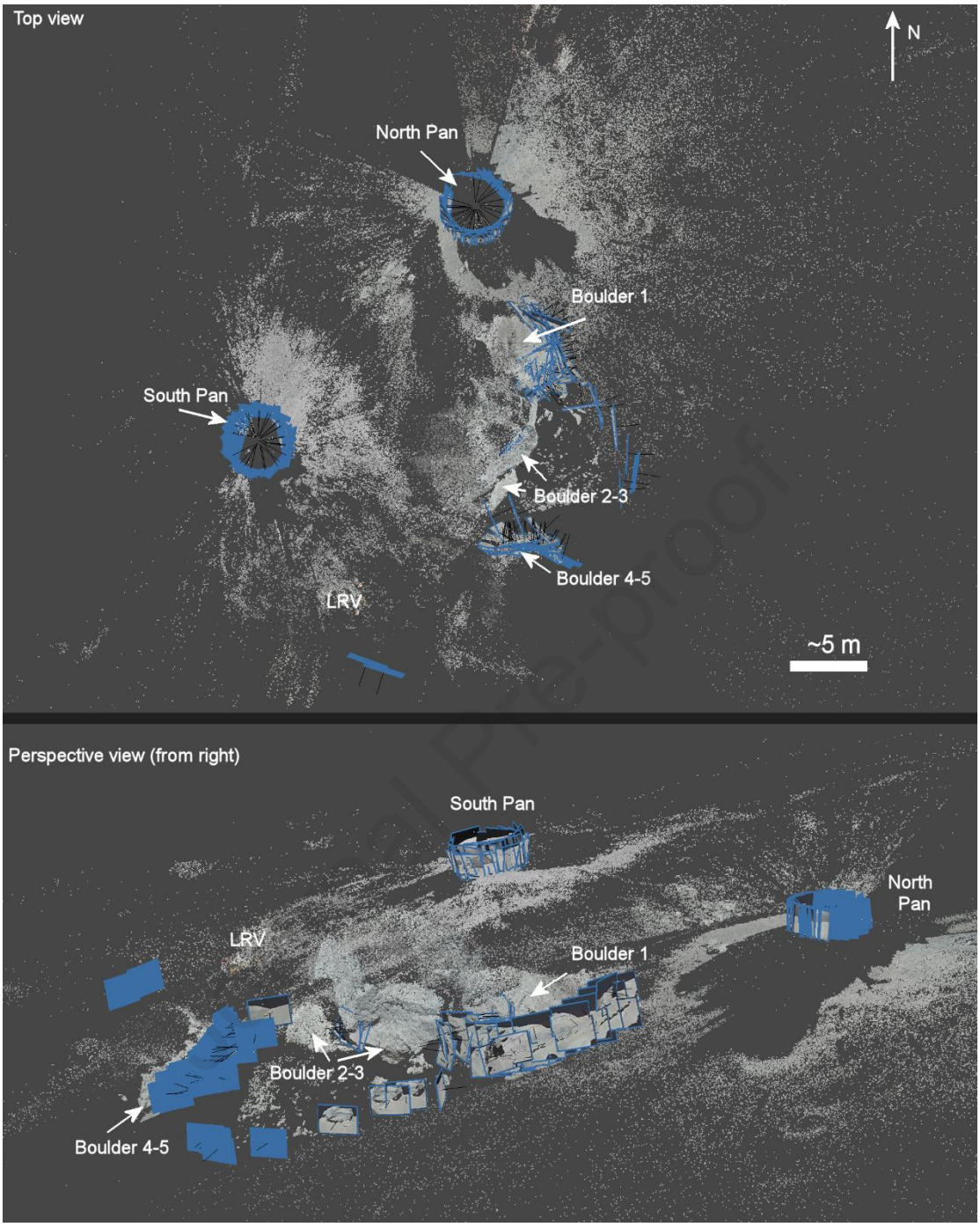

Figure 4: Top view and perspective view (from right to left) of the tie point cloud in the photogrammetric project of the entire Station 6 area. Each of the 154 photographic frames taken by the astronauts appears as a blue rectangle and can therefore be relocated in absolute position.

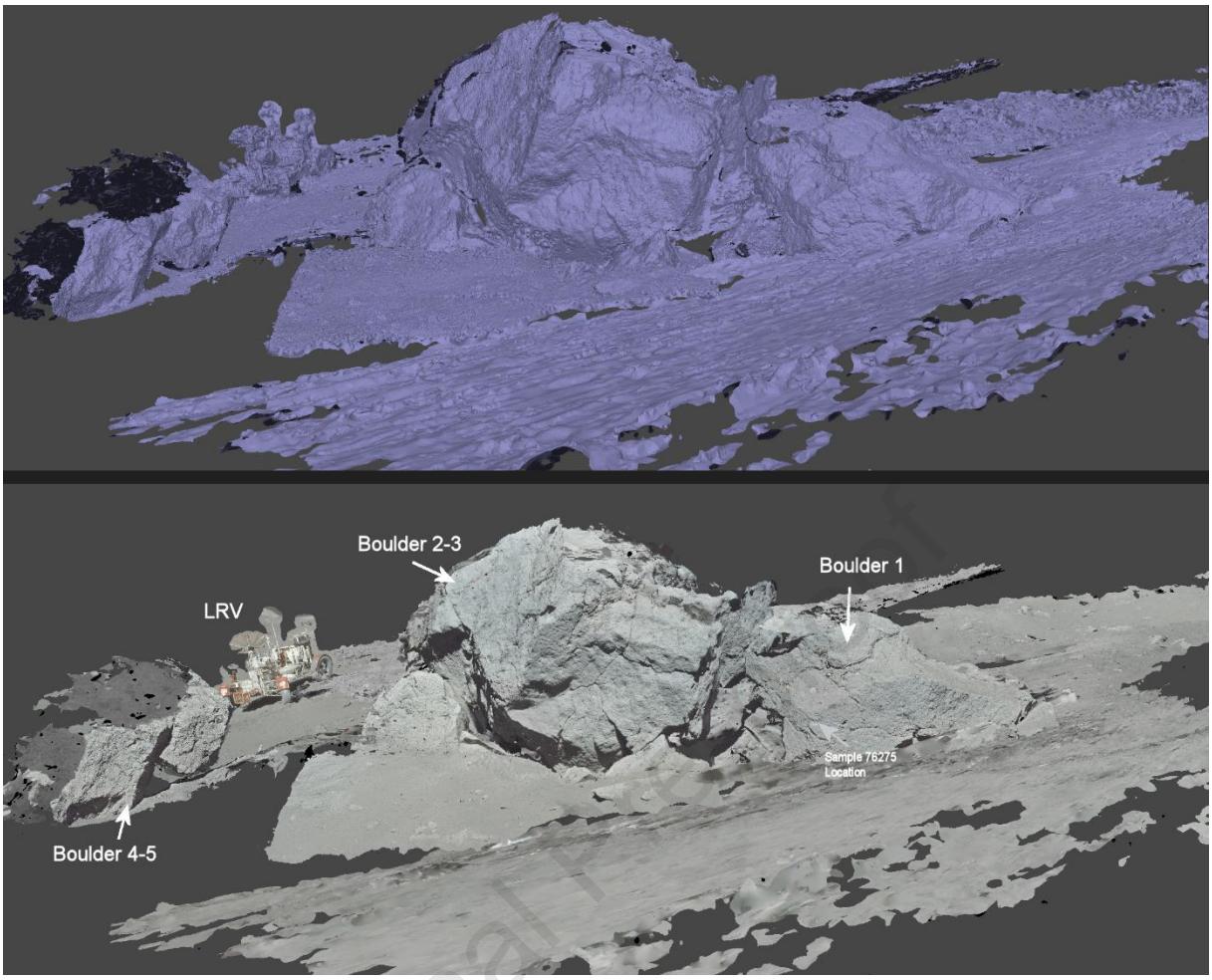

Figure 5: Perspective view of the 3D reconstruction of the main boulders of Station 6. The upper panel corresponds to the solid polygonal mesh. The bottom panel shows the textured 3D model of Station 6.

2.3 Comparison with LRO orbital imagery

Station 6 has been observed in several Lunar Reconnaissance Orbiter NAC images, acquired vith a wide range of illuminating and viewing conditions. Figure 6 displays nine NAC observations which cover the most extreme incidence angles conditions, and with slew angles ranging between -20° and +15.14°. These images are not orthorectified. This can induce small apparent deformations of the boulders shape either in the right/left direction depending on the slew angle, or in the North-south direction, considering that the boulders are located on a north-south slope of 22.5°. The difference in illuminating and viewing conditions reveals various surface features, such as small impact craters, the boulders track, and more importantly some parts of the astronauts footprints. Various parts of the footprints are particularly showing up in images M129086118LR, M109032389L, M172717297R, and M113751661LR. These footprints can serve as a test for the validity of the photogrammetric reconstruction that we discussed in the previous section. Indeed, the positions of the images derived from photogrammetry should logically fall withing the astronauts footprints revealed by LRO. This is indeed what we can observe in Figure 7, where the photogrammetric project has been superimposed on the LRO image M129086118LR. This LRO image has been taken with a slew angle of 0°, therefore minimizing possible East-West apparent deformations of the boulders. We see for example that the dark footprint markings on LRO correspond to the derived location of the seven images acquired to characterize Boulder 2-3, on the right side of the figure. We also see in figure 7 that the location of the North panorama taken by G. Cernan falls at the top end of the dark markings on LRO, which also validates their derived location. The position of the photographs and the contour shape of the boulders seem to generally agree with the LRO background by less than ~1m (one subdivision of the grid), a value that we consider as a conservative estimate of the accuracy of the reconstruction.

The LRO coverage of the Station 6 covers a moderately wide range of illuminating and viewing conditions, potentially also opening new fields of research using orbital images. In further studies, control points could be collected from the orthorectified LRO NAC images to help in solving more easily and accurately the position, scale and orientation of the photogrammetric reconstruction using scanned Apollo film photographs. We used the Astropedia USGS orthorectified mosaic (0.5 m/pixel) and its associated DEM (1.5 m/pixel) processed from NAC

stereo pairs to evaluate the interest of doing orbital photogrammetry. However, it turns out that the 1.5 m spatial resolution of the DEM is not really high enough to accurately sample the shape of the boulders, which represent less than 5 pixels each in their largest dimension in the DEM. Consequently, they only appear as a smoothed bump in the USGS DEM. A detailed study of the potential of orbital images to derive the 3D shape of the boulders would probably require the use of more sophisticated approaches such as the subpixel-scale topography retrieval and Super-resolution techniques developed by Tao et al. (2022). Alternatively, a shape-from-shading approach would also be potentially useful to derive pixel-level resolution DEM using monocular LRO images, as developed by Wu et al. (2018). These approaches fall beyond the scope of our study which was mainly focused on ground data. We therefore decided to leave the systematic study of the set of LRO NAC orbital images with state of the art algorithms to further integrated works.

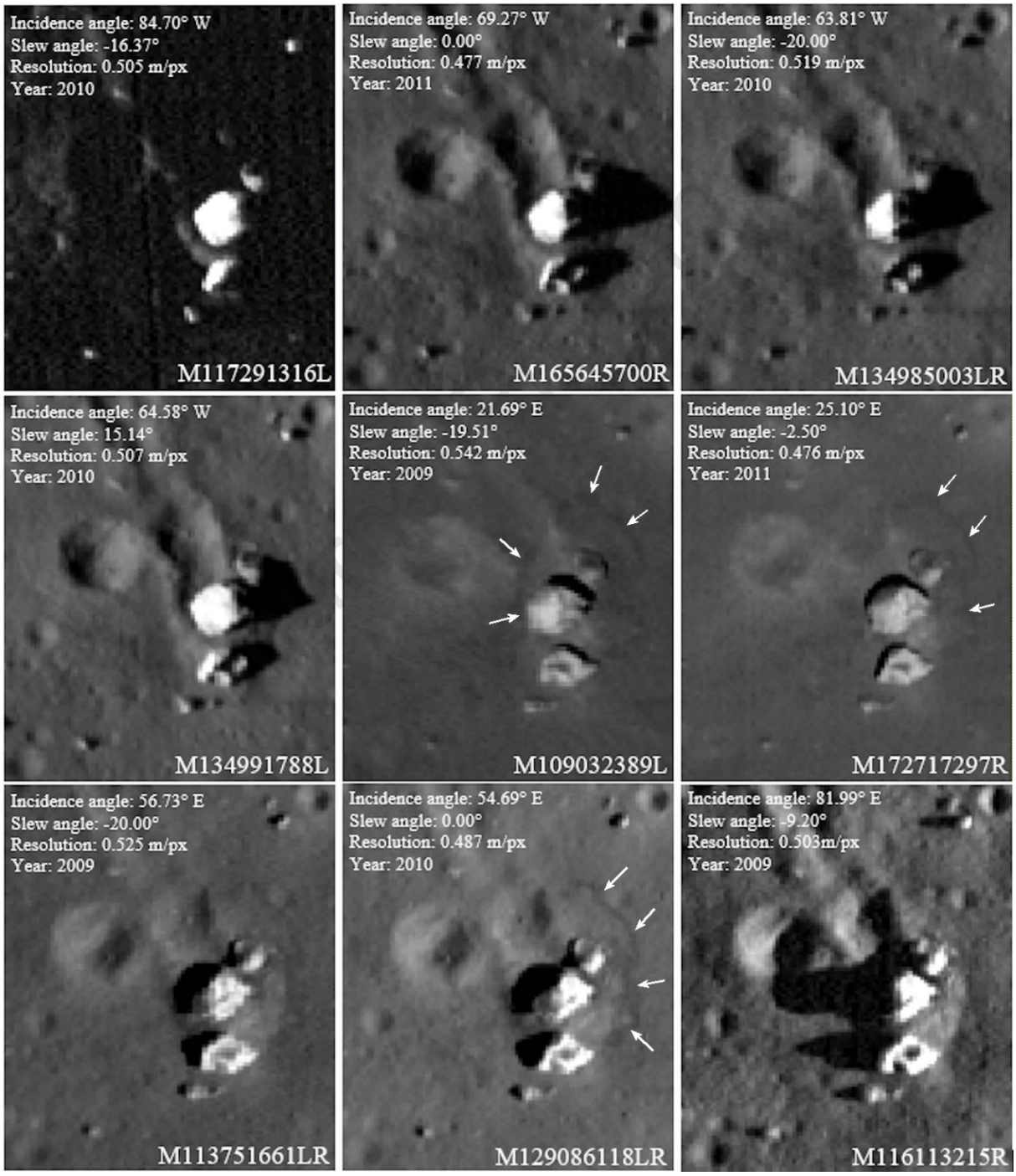

Fig 6: LRO NAC images of the station 6 area, showing the boulders seen with a wide range of illuminating (incidence angle) and viewing (slew angle) conditions. The difference in illuminating conditions reveals small craters, the boulders track and

also part of the astronaut footprints, which appear as a dark line of disturbed soil, in particular in images M129086118LR and M109032389L (arrows).

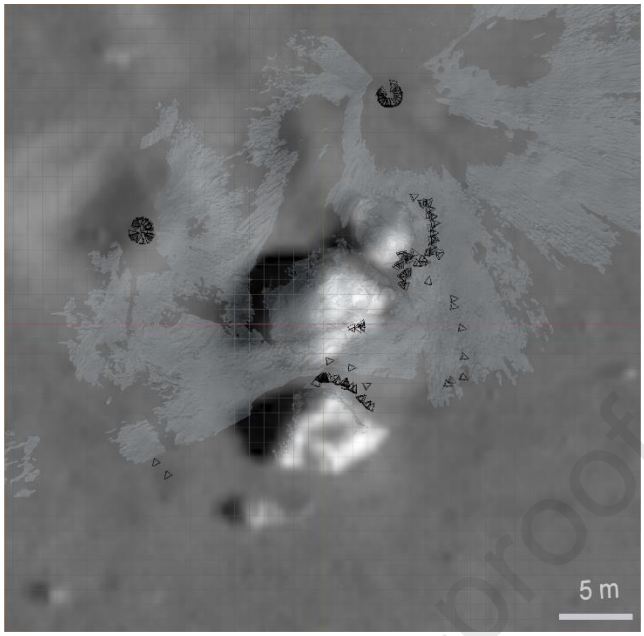

Fig. 7 : Superposition of the photogrammetric model over the LRO image M129086118LR. The location of photographs (in particular on the right part) falls within the dark footprint markings. The North Pan appears also connected to the disturbed soil markings.

3 - Photogrammetric 3D reconstruction of the Station 6 rock samples brought back to Earth

In addition to the 3D reconstruction of the boulders and part of their surroundings, we pushed the process one step further by reconstructing the rock samples themselves. To this end, we took advantage of the fact that the rock samples retrieved from the boulders were thoroughly documented in the Lunar Receiving Lab in Houston once brought back on Earth. In our study, we used as input series of original scanned photographs available on the Lunar and Planetary Institute website. Up to 16 stereoscopic photographic pairs were systematically acquired for a significant number of the samples placed on a rotating stage, with 8 pairs evenly ordered in the equatorial plane of the sample and 8 other pairs evenly ordered on a roughly perpendicular plane. Two examples of such input images are shown in Figure 8 for sample 76015.

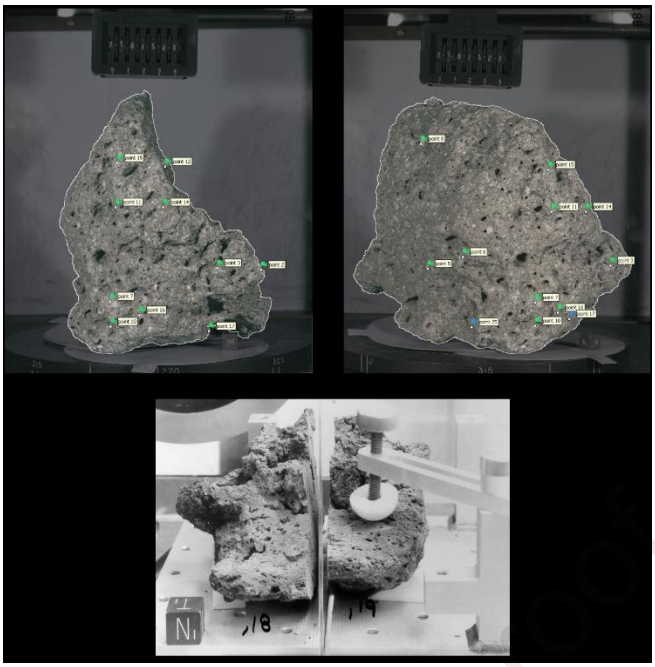

Figure 8: Example of archived laboratory photography's of rock sample 76015 taken from Boulder 5. Samples were systematically photographed from different angles during the seventies. Up to 16 pairs of stereoscopic images are available for a significant number of samples. During the photogrammetric reconstruction process, we added markers manually on each image to facilitate the image alignment steps. These images can serve as the basis to compute a complete 3D numerical model of the rocks (see Figure 9) before they were eventually sawed in multiple pieces, as shown on the bottom image S76-21672 of sample 76015 taken after being saw cut at the Lunar Receiving Laboratory in 1976.

Samples were photographed on a rotating stage with a fixed background displaying the sample number and a 1-cm cube included for scale. We used masks corresponding to the detouring of the rocks to avoid correlation errors induced by the fixed background during the computation of the sparse tie points cloud. When a sufficient number of viewpoints is available, the set of photos potentially allows a complete photogrammetric 3D reconstruction of the rocks using the Structure from Motion technique. This technique is also used in the Astromaterials 3D for samples which can still be photographed today (Blumenfeld et al., 2015). Rock samples at Station 6 have been sawed in multiple pieces for analysis, and are therefore not available anymore in their pristine form for a new photographic characterization campaign. One must therefore only rely on the available archived images. Depending on the complexity of the shape of the rocks, the significant angle difference of ~45° between each stereoscopic viewpoint sometimes prevents the photogrammetric software to automatically find tie points during the first image alignment step. In most cases, we therefore had to manually add several markers on the original photographs to help the algorithm to converge (Figure 8). Before the final texture generation step, we applied a first order color balance of the scanned photos in order to homogenize their illuminating conditions, which was not always fully coherent within series of images. By using these preliminary steps, we were finally able to compute a detailed textured 3D model for each of rock samples 76015, 76215, 76315 and 76275.

3.1 Sample 76015

This rock sample 76015, which was loose and in place on Boulder 5, was lifted off the top corner of Boulder 5. It was photographed before and after being removed. It is a large, 2.8 kg sample of tan-gray, vesicular, micro-poikilitic, impact melt-breccia (Wolfe et al., 1981). It shows an exposed surface with a thin brown patina locally penetrated by micrometeorite impact craters, a dark area without microimpacts at its edge, and a partially protected fresh lighter zone (Meyer, 2008; 2010). It is a metaclastic (ground up and recrystallized) breccia with the originally melted fine-grained matrix now made up of interlocking crystals of pyroxene that enclose small plagioclase crystals (poikilitic texture). A wide variety of lithic and mineral clasts exists in the rock, including various combinations of plagioclase, pyroxene, orthopyroxene, and olivine as well as basalt (Schmitt, 2022). Radiogenic dating using ^{40}Ar-^{39}Ar technique indicates a crystallization age of ~3.9 billion years (Turner and Cardogan, 1975; Cadogan and Turner, 1976). Schmitt, et al. (2017) interpret the age to be ~3.92 Gyr. The exposure age derived from a ^{81}Kr-Kr technique probably indicates the moment when the boulders fell down of North Massif. It is estimated at 17.5 ± 0.5 Myr. (Crozaz et al., 1974).

We used 32 archived images labeled S73-18763 to S73-18778 to carry out the photogrammetric 3D reconstruction process. These images were taken before the sawing of the sample in multiple pieces for various

scientific investigations. All images were aligned using 60 markers in order to produce a final textured 3D model of 800.000 polygons. The different steps of the reconstruction are illustrated in Figure 9. The 3D model of this rock, which does not exist anymore in this pristine form, can be freely manipulated online at https://sketchfab.com/LPG-3D/collections.

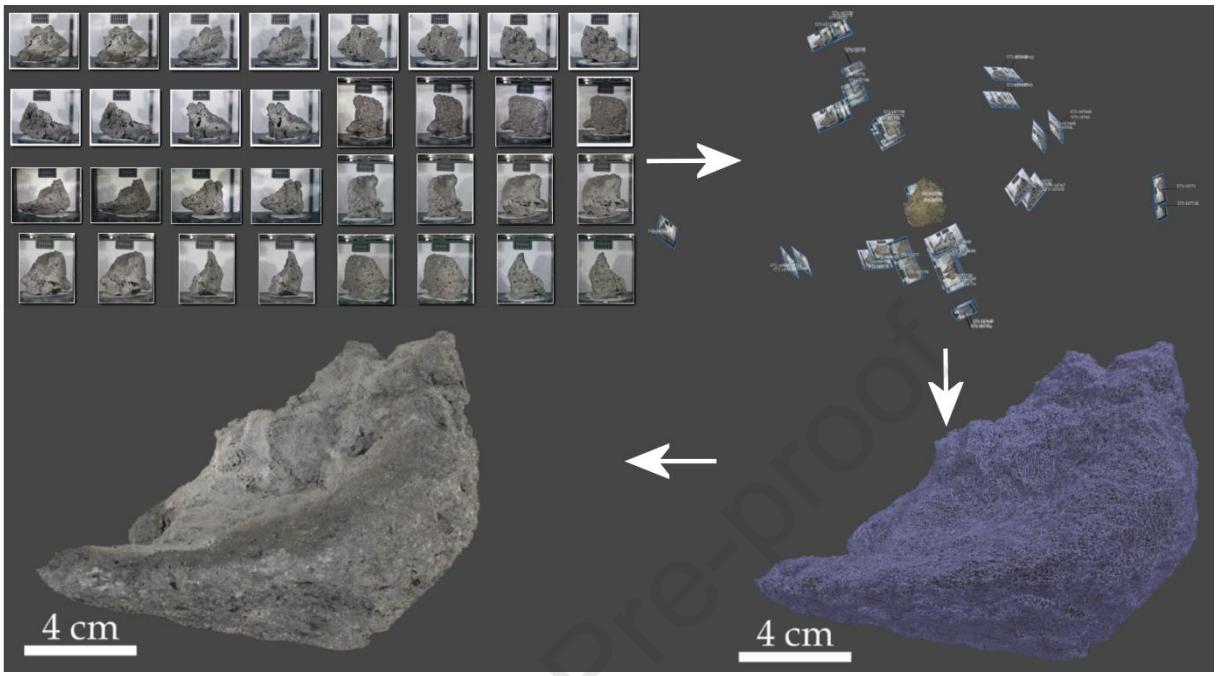

Figure 9: Photogrammetric 3D reconstruction of rock sample 76015 using 32 archived laboratory images labeled S73-18763 to S73-18778 as input (upper left). All images were aligned in the Agisoft Metashape software (upper right), to produce a 3D mesh (lower right) that has been textured with a mosaic of original images (lower left). The 3D model of this rock, which has been sawed in multiple pieces and therefore does not exist physically anymore in its original form, can be viewed and manipulated online at this address: https://sketchfab.com/LPG-3D/collections.

3.2 Sample 76215

The spalled rock sample 76215 has been taken at the base of Boulder 4, where it was coincidentally lying next to the gnomon. This sample, similar to 76015, consists of a vesicular micropoikilitic impact melt breccia with a few small, plagioclase-rich rock (lithic) clasts and plagioclase and olivine mineral clasts. It presents an exposed, patina-covered surface with micrometeorite impact craters and multiple protected areas (Meyer, 2010). The matrix is a poikilitic intergrowth of plagioclase and olivine in larger clinopyroxene (pigeonite and augite) crystals. The poikilitic texture grades to ophitic (laths of plagioclase in pyroxene) near the walls of vesicles. The plagioclase clasts have euhedral (showing crystal faces) overgrowths (Schmitt, 2022). Radiogenic dating using the ^{40}Ar-^{39}Ar technique indicates a crystallization age of the matrix of ~3.94 billion years (Cadogan and Turner, 1976). An exposure age derived from the ^{81}Kr-Kr technique was estimated at ~19 million years.

As for the previous sample, a set of 32 scanned archived photography's (16 stereoscopic pairs, labeled S73-20410 to S73-20425B) are available for the 3D reconstruction process. For this sample, all images were correctly aligned without the need of adding any manual tie point. This is due to the relative simple convex geometry of the sample. Figure 10 shows the result of the photogrammetric pipeline. The 3D model can freely be manipulated to investigate the respective properties of the exposed versus protected surfaces of the rock.

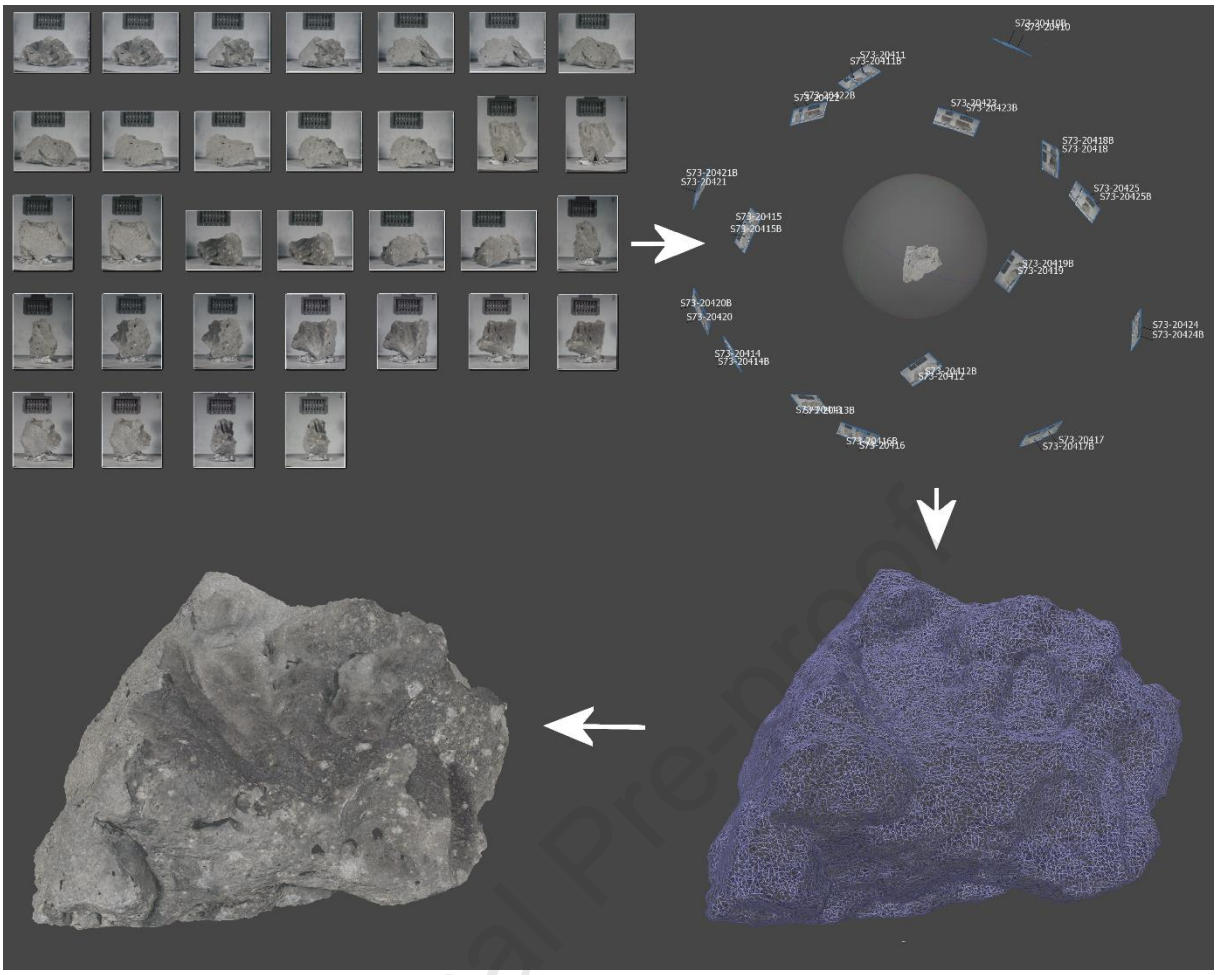

Figure 10: Main steps of the 3D reconstruction process for sample 76215. 32 original photos of the sample (upper left) are aligned into the photogrammetric software (upper right). The automated correlation between overlapping images is used to produce a 3D mesh (lower right). A final draping texture is computed using a mosaic of the original photos (lower left). This model can be viewed and manipulated online at this address: https://sketchfab.com/LPG-3D/collections

3.3 Sample 76315

This rock sample 76315 has been extracted from boulder 2 at Station 6. It corresponds to an impact melt breccia, composed of an exposed, patina-covered surface with micrometeorite impact craters and a partially protected fresh zone (Meyer, 2010). This breccia contained two important clasts, a feldspathic granulite clast and an anorthositic clast. The large white plagioclase-rich clast is veined by impact melt that is now very finely crystalline. The blue-gray portion of 76315 is very finely vesicular (vesicles less than 1 mm across) and very fine crystals of olivine and pyroxene enclose plagioclase. Lines of vesicles define a consistent foliation through the sample (Schmitt, 2022). Radiogenic dating made on this sample using ^{40}Ar-^{39}Ar technique indicates a crystallization age of the blue-gray matrix of ≈3.9 Byr (Turner and Cadogan, 1975). This is probably the age of the Crisium basin-forming event (Schmitt et al., 2017). Its exposure age estimated from a ^{81}Kr-Kr technique is ~22 ± 1 Myr (Crozaz et al., 1974). Figure 11 shows the result of the 3D reconstruction process of sample 76315 that we carried out using 32 scanned archived images corresponding to 16 stereoscopic pairs, labeled S73-18731 to S73-18746B.

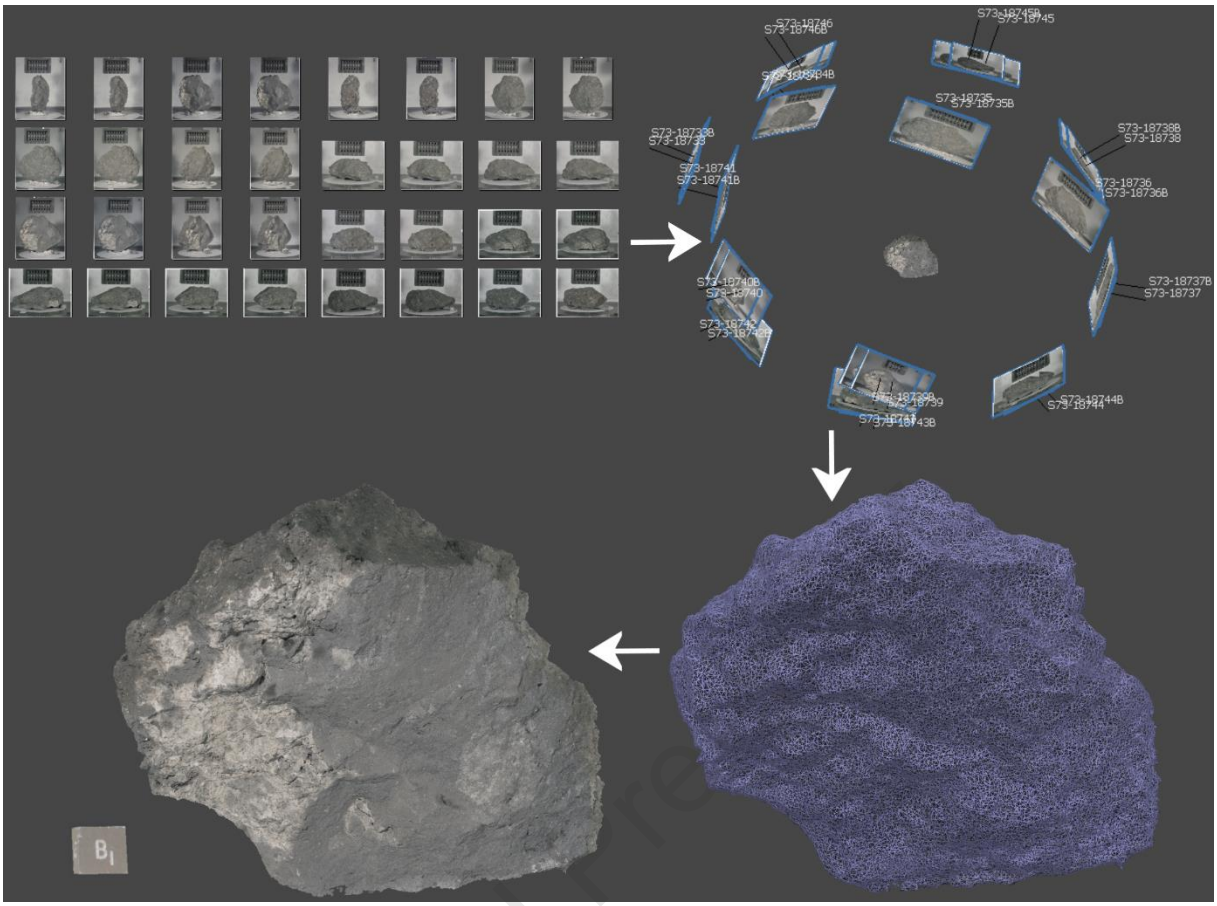

Figure 11: Main steps of the 3D reconstruction process for sample 76315. 32 original archived photos of the sample (upper left) are aligned into the photogrammetric software (upper right). The automated correlation between overlapping images is used to produce a 3D mesh (lower right), textured with a mosaic of the original photos (lower left). The 1-cm cube is provided for scale. This model can be viewed and manipulated online at this address: https://sketchfab.com/LPG-3D/collections

3.4 Sample 76275

The 4.6-cm lunar sample 76275 has been chipped off of the side of boulder 1 (Wolfe et al., 1981). It is a clast-bearing impact, non-vesicular, blue-grey melt breccia, similar to other samples of Station 6 (Meyer, 2012). The modal mineralogy of 76275 is about 50% plagioclase, 40% low-calcium pyroxene, with minor amounts of augite, olivine, ilmenite, armalcolite, and metallic iron. The matrix is finer-grained than for the other samples of the large boulder. Cadogan and Turner (1976) determined an Ar plateau age of 4.02 ± 0.04 b.y. for this sample. Higuchi and Morgan (1975) noted that the trace siderophile element composition of all the samples of the boulders of Station 6 form a tight grouping (meteorite group 2) on compositional diagrams. The sample 76275 has a higher abundance of these meteoritic elements than the matrices of the samples 76015 and 76215. Figure 12 shows the result of the photogrammetric reconstruction process of sample 76275, computed using a set of 38 archives images (images labeled S73-15076 to S73-24039B), taken before the sample was sawed in several tens of pieces for analysis.

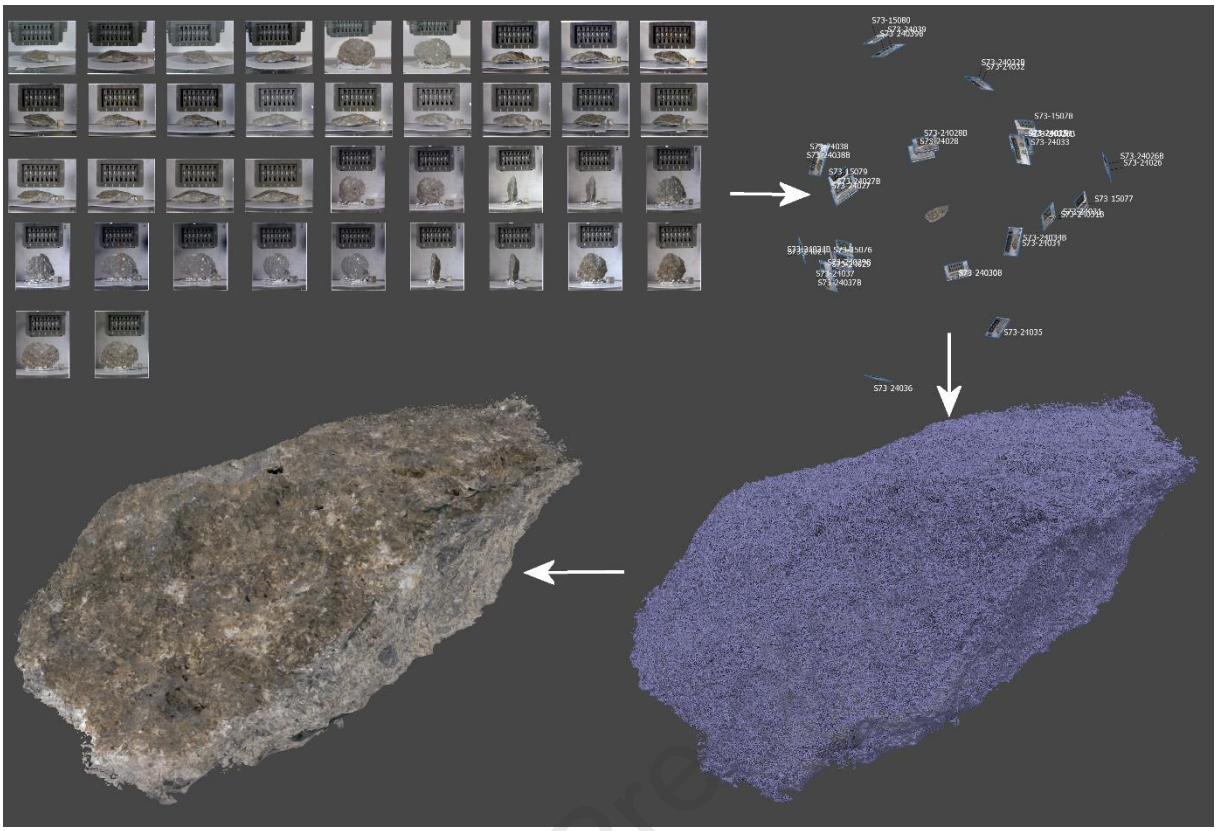

Figure 12: Main steps of the 3D reconstruction process for sample 76275 extracted from boulder 1. 38 original archived photos of the sample (upper left) are aligned into the photogrammetric software (upper right) to produce a 3D mesh (lower right), textured with a mosaic of the original photos (lower left).

3.5 Rock samples 76255, 76295, and 76235

Three other rock samples of Station 6 (number 76255, 76295, 76235) have been brought back to Earth and documented. Sample 76235 also has 16 image pairs, but the alignment did not work, probably due to the lack of texture on this tiny bright rock. Only 16 views (with no stereoscopic pair) were originally available for samples 76295 and 76255 on the LPI website. After investigation, old stereoscopic pairs have been found, but the reconstruction process still did not converge. In the next section, we discuss how the reconstructed rock samples and boulders can be integrated in augmented or virtual reality, and how a first interpretative approach concerning the surface processes can be derived from the constrained orientation of the rocks.

4 Integration in augmented or virtual reality and scientific outcomes

4.1 Availability of the samples on the Sketchfab Plateform

We have posted the 3D models of the rock samples on the Sketchfab web platform at https://sketchfab.com/LPG-3D/collections to allow their easy visual inspection and manipulation. These 3D models are of particular interest considering the fact that these lunar samples have been sawed into multiple pieces after being photographed several decades ago. Therefore, they do not exist anymore in their original physical form, as they have been cut for distribution in curation facilities and modified for destructive analyses. The numerical 3D reconstruction makes them available again for a visual morphological and textural investigation. The 3D numerical model can therefore be thought as a kind of historical preservation of the original rocks. Using this reconstruction, we can eventually obtain a physical copy of the shape of the rocks using a 3D-Printer (Figure 13a, b). They can also be manipulated in virtual reality using a VR headset, or even be viewed using augmented reality with a cellphone or a tablet (Figure 13c, d).

Our study shows that the process can be applied to old archived silver photographs, provided that the number of viewpoints is sufficiently high with respect to the complexity of the shape of the sample. This approach is complementary to the more comprehensive Astromaterials 3D initiative, which is aimed at merging photogrammetric models with X-ray computed tomography data, in particular for samples that are still available

in their pristine form for an in-depth photographic characterization (Blumenfeld et al., 2015; Blumenfeld et al., 2019). In Blumenfeld et al. (2015), up to 240 images taken with increments of 15 degrees at several elevations were used to reconstruct the lunar sample 60639 of the Apollo 16 mission. This is obviously more favorable than the set of 32 archived images separated from 45° that is available on the LPI website for old pristine rocks. Despite this difference, our conclusion is that the process is still achievable in some cases with the set of old images.

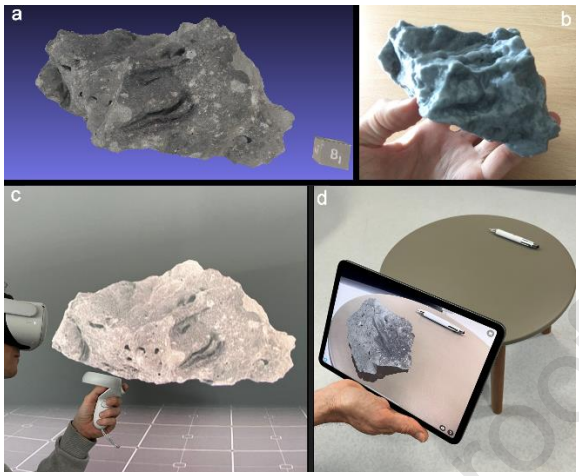

Figure 13: 3D numerical model (upper left) of the lunar sample 76215 compared with its 3D print at 1:1 scale (upper right). The 3D numerical model can also be viewed either in virtual reality (lower left) or in augmented reality (lower right) directly on Sketchfab.

4.2 Repositioning the rock samples in their original position and Virtual Reality simulation

The numerical 3D reconstruction provides the possibility to replace the rock samples at their original position and orientation directly on the 3D models of the boulders themselves. This can be interesting to retrieve the precise original orientation of the samples, to investigate for example the characteristics of their coatings. Several samples show various degree of surface alteration, depending on their exposure to micrometeorite bombardment and solar wind particles. Figure 14 (top left) corresponds to the Apollo images taken before (AS17-140-21411, in the inset) and after (AS17-140-21413) sampling of rock 76015. These before and after images are very useful to constrain the orientation of the 3D model of the sample, which is shown in the upper right of Figure 14. The bottom part of Figure 14 shows the prototype of a simple scene recreated in Virtual Reality using the SteamVR Workshop environment. Whereas more complex simulations can be computed using game engines, this SteamVR environment provides basic functionalities allowing a simple virtual immersive exploration in collaborative mode. We created a simple Steam VR demonstration scene using Boulders and rocks 3D models, which were integrated with Kaguya and LRO orbital imagery to provide the general context (distant horizon). In Figure 14 (bottom part), we see the 3D model of sample 76015 repositioned at the right place and orientation on the 3D model of Boulder 5. Another example is shown figure 15 where the 3D model of sample 76275 is replaced at its original position on the 3D model of Boulder 1. Users equipped with a VR headset can potentially freely evolve in the scene in a collaborative mode (i.e. several users can see each other on the forms of avatars and discuss directly around the boulders), and ultimately investigate the position of the rocks with respect to their parent boulders. Such a VR experience generally allows the user to better understand the real size and characteristics of the geologic features. More generally, VR can also help to give a better sense of distances, which are hard to apprehend on the Moon (or Mars) due to the lack of known reference features and the absence of atmospheric scattering. Samples can be investigated in their real context. It also provides a simple way to examine a given outcrop from any desired point of view (independently of the original pictures). This can be particularly useful to compare the shape and internal structure (e.g., magmatic fabric, fractures, etc.) of the boulders with the information derived from the low-resolution video acquired from the LRV camera viewpoint during the sampling phase. In rare instances for the Moon, this procedure can assist in providing orientations for paleomagnetic studies.

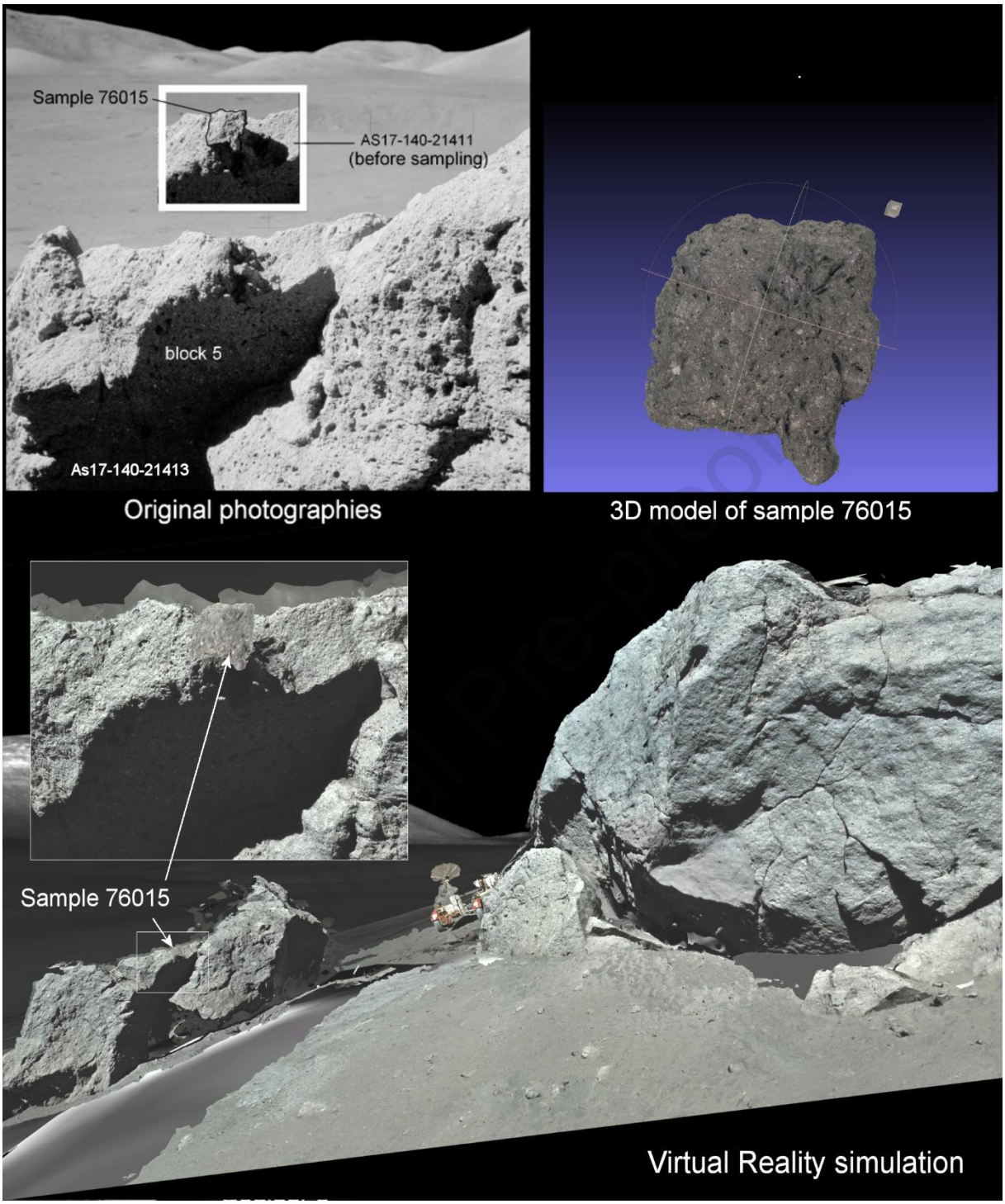

Figure 14: Top left: Original Apollo photos taken before (inset, AS17-140-21411) and after (AS17-140-21413) the removal of sample 76015. Top right: 3D model of sample 76015 derived from laboratory photos. Bottom panel: Virtual reality simulation of station 6 integrating 3D models. Orbital imagery has been used to provide the context. The viewpoint shows boulders 2-3, 4 and 5. Sample 76015 has been placed at its original orientation and location on boulder 5. This scene is accessible at https://steamcommunity.com/sharedfiles/filedetails/?id=2676700770.

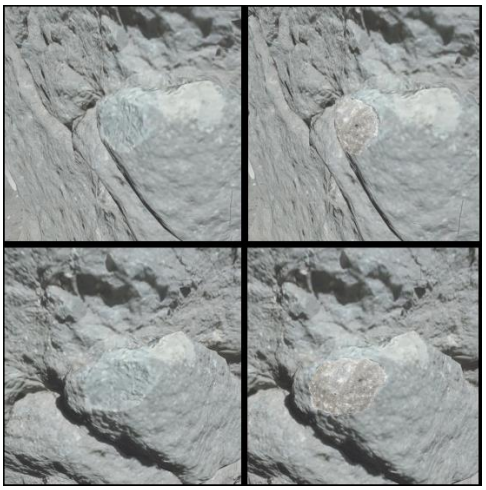

Figure 15: Close-up view of the 3D model of the 4.6 cm-wide sample 76275 replaced at its original location (on right panels) on the 3D model of Boulder 1 at Station 6 (see the context in Fig. 2, red rectangle). The color balance is different due to different illuminating conditions of the sample (in the lab) and the boulder (on the Moon).

4.3 Example of the outcomes : Implication on the study of space weathering processes

Lunar samples were analyzed on Earth, but their interpretation in terms of primary origin (magmatic flows, vesicles, etc.) and alteration processes (space weathering, microcraterization, etc.) requires a knowledge of the orientation and position of these samples in the outcrop. Several studies have carried out such analyses only qualitatively from digital images taken by astronauts. Yet modern techniques of 3D reconstitution can help to provide a more precise localization and orientation of rocks within outcrops. A possible outcome of such a 3D simulation is the study of space weathering processes. On sample 76015, at least three different units at the surface show various degree of patina formation, which can be correlated with the original position of the sample with respect to different levels of exposure impact from micro-meteors and solar wind particles (Figure 16). The upper sky-facing side is the most affected by space weathering effects, with a well-developed patina and small fresh impact craters appearing as small distributed white dots. Interestingly, the VR simulation suggests that one surface of sample 76015 was protected from micrometeorite bombardment, and developed a thick dark patina in a face which appears to be protected by a crevice. This particular setting might be the driving factor of the observed difference in degree of surface alteration, compared to the fresh part of the rock and the highly altered upper face. The thick patina could result from glass splashes on opposing adjacent boulder surfaces (Meyer, 2008). A similar, continous variation in patina thickness is present on the vesicle wall on 76215. Analysis is continuing relative to the variations of patina thickness versus length of exposure, as there are suggestions that Boulders 4 and 5 were broken off Boulder 2 long after the parent boulder rolled into place ~20 million years ago (Schmitt, 2023). Detailed study also may be able to determine if portions of the patina developed before the boulder was dislodged from its bedrock position on the North Massif. If so, oriented paleomagnetic measurements would be possible.

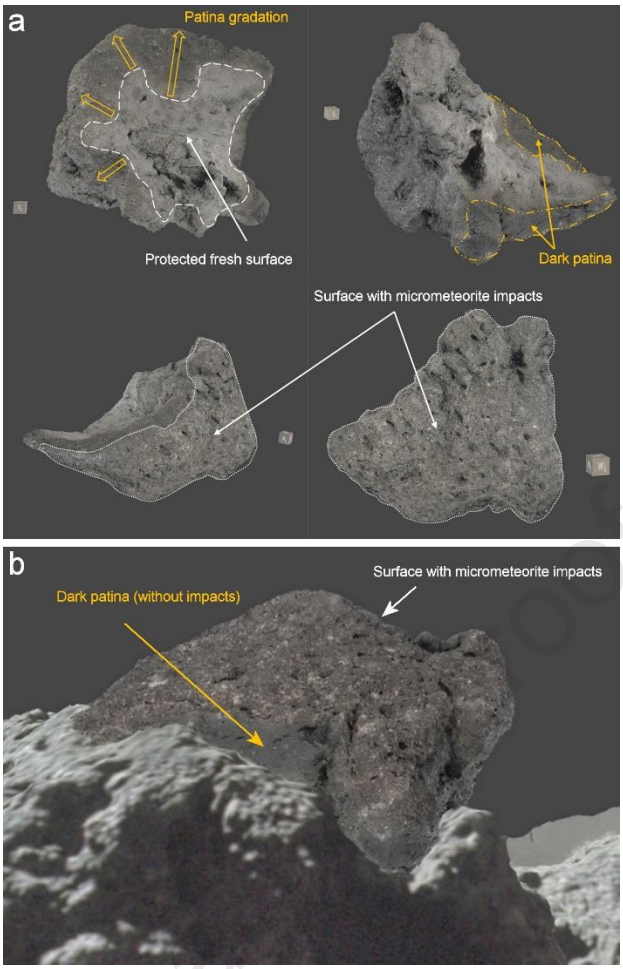

Figure 16 : (a) Multiple 3D views of sample 76015 showing three main units: an altered surface with micrometeorite impacts, a dark patina without craters at its edge, and an underlying fresh light surface. (b) 3D perspective view of the sample replaced on the 3D model of Boulder 5. The thick dark patina area at the bottom of the sample falls in a crevice. The patina could result from glass splashes on opposing adjacent boulder surfaces.

The knowledge of the 3D shape of the boulders also might be useful to simulate the lighting conditions (shadows) with respect to the Sun position during the lunar days, and to identify cold traps. Regolith sample 76240 was collected under the base of Boulder 4's North face in a continuous shadowed area, whereas regolith sample 76260 was collected in a nearby sunlit part of the soil. Differences in thermoluminescence states have been noted between such Sun-protected versus Sun-illuminated regolith samples (Schmitt, 2023; Sehlke and Sears, 2022), distinguishing the role played by energetic solar wind and internal alpha particles in maturation processes (Schmitt, 2023).

5 Conclusion and perspectives

We have reconstructed the Station 6 boulders and rock samples of the Apollo 17 mission using Structure From Motion photogrammetry techniques that employ a set of archived scanned silver photographs as input. We show in particular that both boulders documented in the field and lunar rock samples imaged in the lab can be investigated by this technique. The reconstruction process worked well despite the use of scanned silver films instead of a digital camera, as is most often the case with photogrammetry nowadays. It was made possible by the operational strategy employed by the astronauts, who documented the outcrops by using stereoscopic views before and after sampling, most often with a significant overlap between images. The boulders of Station 6 were reconstructed using all the available imagery, representing a set of 154 aligned Apollo images. Four of the six rocks retrieved from these boulders were also reconstructed in 3D using sets of 32 archived images from the LPI for each of the samples. The 3D numerical models of lunar boulders and rock samples can serve both for scientific analysis, education and outreach. They also play a role in the preservation of a cultural heritage. Indeed, several lunar rock samples have been sawed in multiple pieces for analysis and do not exist anymore in their original form.

The 3D numerical reconstruction derived from archived stereoscopic images makes them potentially available again for a visual investigation. The process illustrated in this study can be generalized to the investigation of other samples archived at the LPI, provided that the 16 stereoscopic pairs are also available. For rock samples that are still available today, a higher number of images would be preferable for a more precise 3D scan. Blumenfeld (2015) used 240 images for a single Apollo 16 sample. From lab experiments, an empirical recommendation would be to take images of the sample on a rotating stage by steps of ~15° horizontaly with both a side view and a view at ~45° taken at each step, and to repeat the process on at least 2 or 3 different orthogonal positions of the rock to get both sides. The photogrammetric reconstruction can also be carried out in other landing sites (Pustynski, 2021). On Station 6, new photogrammetric studies might possibly be conducted in the future in order to further evaluate the benefit of using a different calibration of the two cameras in the photogrammetric processing of this specific data set, and using possible additional constrains derived from super-resolution studies of orthorectified LRO NAC images. Similarly, other photogrammetric chains such as Reality Capture might also be tested in order to compare the results with the one obtained with Agisoft Metashape.

Several lunar robotic and even human missions are planned in the coming years. It will be of great interest to image the lunar surface features from different viewpoints and with enough overlap between images during these missions, in order to more routinely reconstruct the explored environment in 3D, providing the possibility to setup virtual or augmented reality simulations. Such AR/VR rendering will be useful in support of operations on the lunar surface, and can serve as a basis for further scientific, education and outreach investigations. New samples that will be brought back from these mission could also be systematically scanned in 3D using photogrammetry in order to document them in their pristine form and to possibly facilitate their sharing and conservation before being modified for destructive analysis.

Acknowledgment : We are grateful to Ryan Zeigler, Apollo Sample Curator at the NASA – Johnson Space Center, and Bridget Mcinturff-Burt for useful discussions about the availability of lunar samples stereo pairs. We also thank two anonymous reviewers for their very constructive comments.

References :

Allton, J. H., 1989. Catalog of Apollo lunar surface geological sampling tools and containers, NASA/JSC-23454

Blumenfeld, E. H., Evans, C. A., Oshel, E. R., Liddle, D. A., Beaulieu, K., Zeigler, R. A., Hanna, R. D., and Ketcham, R. A., 2015. Comprehensive Non-Destructive Conservation Documentation of Lunar Samples Using High-Resolution Image-Based 3D Reconstructions and X-Ray CT Data. 46th Lunar and Planetary Science Conference.

Blumenfeld, E. H., Beaulieu, K. R., Thomas, A. B., Evans, C. A., Zeigler, R. A., Oshel, E. R., Liddle, D. A., Righter, K., Hanna, R. D., and Ketcham, R. A., 2019. 3D Virtual Astromaterials Samples Collection of NASA's Apollo Lunar and Antarctic Meteorite Samples to be an Online Database to Serve Researchers and the Public, 50th Lunar and Planetary Science Conference.

Borgeson, W. T. and R. M. Batson, 1969. Photogrammetric calibration of Apollo film cameras, USGS report, https://www.lpi.usra.edu/resources/USGS-Reports/Astro-0015.pdf

Cadogan, P. et G. Turner, 1976. The chronology of the Apollo 17 Station 6 boulder, Proc. Lunar Sci. Conf. 7, 2267–2285.

Crozaz, G., R. Drozd, C. Hohenberg, C. Morgan, C. Ralston, W. M. et D. Yuhas, 1974. Lunar surface dynamics - Some general conclusions and new results from Apollo 16 and 17. Proceedings of the Fifth Lunar conference (Supplement 5, Geochimica et Cosmochimica Acta), vol 3, pp 2475-2499.

Favalli, M., Fornaciai, A., Isola, I., Tarquini, S., Nannipieri, L., 2012. Multiview 3D reconstruction in geosciences. Comput. Geosci. 2012, 44, 168–176.

Haase, I.; Wählisch, M.; Gläser, P.; Oberst, J.; Robinson, M., 2019. Coordinates and Maps of the Apollo 17 Landing Site. Earth Space Sci., 6, 59–95.

Higuchi H. and Morgan J. W., 1975. Ancient meteoritic component in Apollo 17 boulders. Proc. Lunar Science Conference 6th., Vol. 2, 1625-1651.

Hurwitz and Kring, 2016. Identifying the geologic context of Apollo 17 impact melt breccias, Earth and Planetary Science Letters, 436, 64–70.

Jones, E.M. 2014. Apollo 17 Lunar Surface Journal, Last accessed: 5 November 2017. https://history.nasa.gov/alsj/a17/images17.html#22355.

Kuehnel, H. A., 1972. Apollo experience report: Photographic equipment and operations during Manned spaceflight programs, Nasa technical note ID19720025202.

Le Mouélic, S., Enguehard, P., Schmitt, H. H., Caravaca, G., Seignovert, B., Mangold, N., Combe, J-P., Civet, F., 2020. Investigating Lunar Boulders at the Apollo 17 Landing Site Using Photogrammetry and Virtual Reality, Remote Sensing, 12 (11), DOI: 10.3390/rs12111900.

Meyer, C, 2008. Lunar sample Compendium,
https://www.lpi.usra.edu/lunar/samples/atlas/compendium/76015.pdf.

Meyer, C., Lunar Sample Compendium, 2010. 41st Lunar and Planetary Science Conference, held March 1-5, 2010 in The Woodlands, Texas. LPI Contribution No. 1533, p.1016.

Meyer, C., 2012. Lunar sample Compendium,
https://www.lpi.usra.edu/lunar/samples/atlas/compendium/76275.pdf

Pustynski, V.-V., Jones, E.M., 2014. Photogrammetry of Apollo 11 surface imagery, J. Br. Interplanet. Soc. (JBIS) 67, 390-398.

Pustynski, V.-V., 2021. Cartography of the Apollo 12 landing site from photogrammetric analysis of surface imagery, Planet. Space Sci., 195, 105133.

Roseborough, T. A.; N. R. Gonzales, A. R. Schoonover, V. Tewary, J. A. Woody, M. L. Bouwens, K. B. Patel, G. Sondrup, R. W. Wagner, M. R. Henriksen, J. R. Leland, M. S. Robinson, Apollo 16 and 17 spatio-temporal traverse mapping, 54th LPSC, The Woodlands, 13-17 March, abstract#2869.

Schmitt, H. H*,* Petro, N.E., Wells, R.A., Robinson, M.S., Weisss, B.P., Mercer, C.M., 2017. Revisiting the field geology of Taurus-Littrow. *Icarus*, *298*, 2–33, doi:10.1016/j.icarus.2016.11.042.

Schmitt, H. H., 2023. Continuously ("permanently") shadowed lunar regolith sampled by Apollo 17: key tests of regolith temperature strorage for Artemis, 54th LPSC, The Woodlands, 13-17 March, abstract#2170.

Schmitt, H. H., 2022. Diary of the 12th Man, <americasuncommonsense.com>, Chap. 12.

Sehlke A and Sears, D. W. G, 2022. Thermal Histories of Lunar Cold Traps: Prospecting for Volatiles by Thermoluminescence, Lunar Polar Volatiles Conference, held 2-4 November, 2022 in Boulder, Colorado. LPI Contribution No. 2703.

Spudis, P. D., and G. Ryder, 1981. Apollo 17 impact melts and their relation to the Serenitatis basin, Proc. Lunar Planet. Sci. Conf., 12th, 133–148.

Tao Y., S. Xiong, J-P. Muller, G. Michael, S. J. Conway, G. Paar, G. Cremonese, N. Thomas, 2022. Subpixel-Scale Topography Retrieval of Mars Using Single-Image DTM Estimation and Super-Resolution Restoration, Remote Sens. 2022, 14(2), 257, doi:10.3390/rs14020257.

Turner, G. and P. H. Cadogan, 1975. The history of lunar bombardment inferred from ^{40}Ar-^{39}Ar dating of highland rocks. Lunar and Planetary Science Conference Proceedings 2, 1509–1538.

Ullman, S., 1979. The interpretation of structure from motion. Proc. R. Soc. Lond. Ser. B Biol. Sci., 203, 405–426.

Wolfe, E.W. et al., 1981. Geologic investigation of the Taurus-Littrow Valley: Apollo 17 landing site. *U.S. Geol. Surv. Prof. Pap*. 1981, *1080*, 225–280.

Wu, B., W.C. Liu, A. Grumpe, C. Wöhler, 2018. Construction of pixel-level resolution DEMs from monocular images by shape and albedo from shading constrained with low-resolution DEM, ISPRS J. of Photogrammetry and Remote Sensing, Vol 140, 3-19, doi:10.1016/j.isprsjprs.2017.03.007

Wu, B., Y. Li, W.C. Liu, Y. Wang, F. Li, Y. Zhao, H. Zhang, 2020. Centimeter-resolution topographic modeling and fine-scale analysis of craters and rocks at the Chang'E-4 landing site, Earth and Planetary Scienc Letters, vol 553, doi:10.1016/j.epsl.2020.116666.

Highlights :

- We use photogrammetry on Apollo photographs to reconstruct in 3D the boulders of the Station 6 of the Apollo 17 mission
- 154 images are integrated into a single photogrammetric project to produce a scaled 3D model of the area and to localize the images, which are in good agreement with footprint markings seen on LRO orbital imagery
- We use archived laboratory images of four lunar rock samples retrieved from Station 6 boulders to also reconstruct the lunar samples in 3D, in their pristine form (before they were saw cut)
- Such 3D models can be used for science, outreach or eduction, and can serve in virtual and/or augmented reality simulations. Models can be viewed online on the sketchfab Web plateform.

S. Le Mouélic: Conceptualization, Methodology, Software, Investigation, Formal Analysis, Visualization, Writing - Original Draft, Writing - Review & Editing. **M. Guenneguez**: Investigation, Methodology, Visualization, Writing - Review & Editing. **H. H. Schmitt**: Resources, Investigation, Validation, Writing - Review & Editing. **L. Macquet**: Investigation, Methodology, Visualization, Writing - Review & Editing**. N. Mangold**: Methodology, Funding acquisition, Writing - Review & Editing. **G Caravaca**: Investigation, Methodology, Writing - Review & Editing. **B. Seignovert**: Investigation, Methodology, Writing - Review & Editing**. E. Le Menn**: Resources**. L. Lenta**: Resources

Declaration of interests

☒ The authors declare that they have no known competing financial interests or personal relationships that could have appeared to influence the work reported in this paper.

☐ The authors declare the following financial interests/personal relationships which may be considered as potential competing interests: